Heliyon 10 (2024) e39102

Contents lists available at ScienceDirect

Heliyon

journal homepage: www.cell.com/heliyon

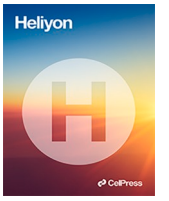

Research article

Piezoelectric barium titanate/hydroxyapatite composite coatings on Ti-6Al-4V alloy via electrophoretic deposition

Akhila S Nair, Leema Rose Viannie *

Department of Physics, School of Advanced Sciences, Vellore Institute of Technology, Vellore, 632 014, Tamil Nadu, India

ARTICLE INFO

Keywords:
Barium titanate
Bioceramics
Electrophoretic deposition
Piezoelectric materials
Raman spectroscopy

ABSTRACT

Electrophoretic deposition (EPD) is a widely accepted, cost-effective and simple method to obtain conformal coatings of dense nanoparticles via application of a DC voltage. This paper reports the physical and mechanical properties of nanostructured barium titanate/hydroxyapatite (BT/HA) ceramic composites coated onto Ti-6Al-4V alloy via cathodic EPD in various ratios of 40:60, 50:50 and 60:40 (HB4, HB5 and HB6) respectively. Homogenous BT/HA coatings were obtained at a notably low voltage of 10 V. The crystallinity and phase analysis confirmed the formation of tetragonal phase of BT indicating the piezoelectric property. HB6 exhibits maximum piezoelectric coefficient (d_{33}) of 159 pC/N and Vicker's hardness of 242.31 HV. The cross-sectional electron micrographs show well connected and homogeneous coatings with increasing amounts of BT. Human mesenchymal stem cell lines were utilized in biocompatibility experiments, which revealed that HB composites had greater viability of HW-MSCs cells than pure BT, with HB6 exhibiting a maximum cell viability of more than 90 %.

1. Introduction

The existence of piezoelectricity in human bone was first reported by Fukada and Yasuda in 1957. They observed that bone tissues produce electrical charges when mechanical pressure is applied [1,2]. The origin of this property is attributed to the unique structure and composition of the human bone at the nanoscale level i.e., the collagen fibres and hydroxyapatite crystals that possess inherent dipole moment [3]. The mechanical responsiveness of bone and the activities of bone cells are impacted by these electrical potentials that match the applied stress. This leads to the concept of introducing an electroactive element into the implant material in order to improve bone remodelling and repair. Implant surfaces should be coated with biomedical ceramic coatings with a high bone-grafting capacity because of the metal implants' limited biocompatibility. Hydroxyapatite (HA), with the chemical formula $Ca_{10}(PO_4)_6(OH)_2$, based coatings are well known in bone treatments, as calcium phosphate is one of the major constituents in the teeth and bone minerals [4]. Nevertheless, coating with HA alone has certain drawbacks, including HA coated implants providing superior bone pinning compared to coating adhesion eventually causing implant failure and low phosphorous melting point in the coating leading to bioactive coating degradation [5].

There is an increasing interest in piezoelectric materials that can mimic the electrical characteristics of natural bones, and further promote bone regeneration and repair. In order to encourage bone regeneration, barium titanate ($BaTiO_3$) is a frequently used lead-free piezoelectric material with high piezoelectric coefficient and biocompatibility [3]. It can produce micro-electric currents that

* Corresponding author.
E-mail address: leemarose@vit.ac.in (L.R. Viannie).

https://doi.org/10.1016/j.heliyon.2024.e39102
Received 8 April 2024; Received in revised form 5 September 2024; Accepted 7 October 2024
Available online 10 October 2024

encourage calcium salt deposition at the site of the bone defect by imitating the stress-generated potentials (SGPs) of natural bone. Thus, native bone that has deformed can provide piezoelectric polarization stimuli, which can modify bone development and repair tissue [6].

Of the several structural configurations of $BaTiO_3$, the tetragonal structure stands as a notableone, where the Ti^{4+} cation is displaced from the centre of the [TiO_6] octahedron and the cation centre is displaced from the anion centre, contributing to net polarization along the [001] edge direction. The degree of tetragonal distortion of the cell structure, or tetragonality (c/a), which is the ratio of the two lattice parameters c and a, is an important characteristic of tetragonal $BaTiO_3$. The standard c/a value for pure crystalline $BaTiO_3$ is 1.011 at ambient temperature, as its Curie temperature is 120 °C. Tetragonality is a widely used indicator that characterizes the ferroelectricity of tetragonal $BaTiO_3$ and is used to calculate the dielectric characteristics of $BaTiO_3$ [7–9].

Plasma spraying, sol-gel, and micro arc oxidation are a few of the methods used to achieve ceramic composite coatings on orthopaedic biomaterial metal substrates [6,10–12]. Of all these methods, the plasma spraying technique has some disadvantages because the coatings produced using it have unstable properties like rapid solidification, uneven composition, melted and decomposed phases, etc., which make them easily detached from surfaces or reabsorbed into the body environment [13]. Electrophoretic deposition (EPD) has been observed to be a simpler method for producing nanostructural deposits from colloidal solutions and an effective way to create ceramic coatings from powder suspensions on conducting substrates. The EPD technology also produces uniform coatings that can be applied to any complex shape and is cost-effective and less time-consuming. L Mohan et al. (2012) have achieved TiO_2/HA coatings over Ti alloy using EPD technique at 30 V for 5 min and obtained uniform coatings [5], but this coating lacks piezoelectric nature which is indispensable for a bone mimicking implant. A composite of HA/BT/chitosan was coated onto 316 L stainless steel by Sinaei et al. (2020) and showed that an increasing amount of BT in the composite leads to increased hardness and corrosion resistance acceptable for bone replacement [14]. However, Ti alloys are preferred for bone implants owing to their excellent corrosion resistance for a long-term use, more biocompatible and light weight compared to stainless steel [15].

In the present work, our objective is to develop a piezoelectric bioceramic composite coating on the Ti-6Al-4V alloy to enhance its bone regeneration capability as an implant. To achieve this, we synthesized piezoelectric barium titanate (BT) using a citrate-assisted sol-gel method and combined it with hydroxyapatite (HA) to create composites. Three compositions in different ratios of BT:HA i.e., 40:60 (HB4), 50:50 (HB5) and 60:40 (HB6) was prepared. These BT/HA nanocomposites were coated on Ti-6Al-4V alloy using a simple EPD technique at a low voltage and for a shorter duration (Fig. 2(a)). Our investigation focused on evaluating the impact of BT on the material and mechanical properties of the coatings, as well as assessing the piezoelectric characteristics of the material.

2. Materials and methods

2.1. Synthesis of tetragonal barium titanate (BT)

The key steps that are involved in the preparation of $BaTiO_3$ nano powder using citrate assisted sol–gel method are as follows (Fig. 1). To begin with, titanium isopropoxide was mixed and stirred with acetylacetone for 10 min using a magnetic stirrer. Then, citric acid was dissolved in 100 mL deionized water and added to the titanium precursor solution and stirred for 30 min. Suitable amounts of barium nitrate and citric acid were dissolved in deionized water separately, and added to the above solution and stirred for 1 h at 40 °C. Then, the pH (~6.5–7.0) of the solution was maintained by adding ammonia solution (34 %) drop by drop at constant stirring. The temperature was raised to 100 °C at which water started evaporating and leading to the formation of viscous yellow colour gel. The slightly burnt gel was further heated to 150 °C using a hot air oven, and at this stage, the gel started burning leaving behind a

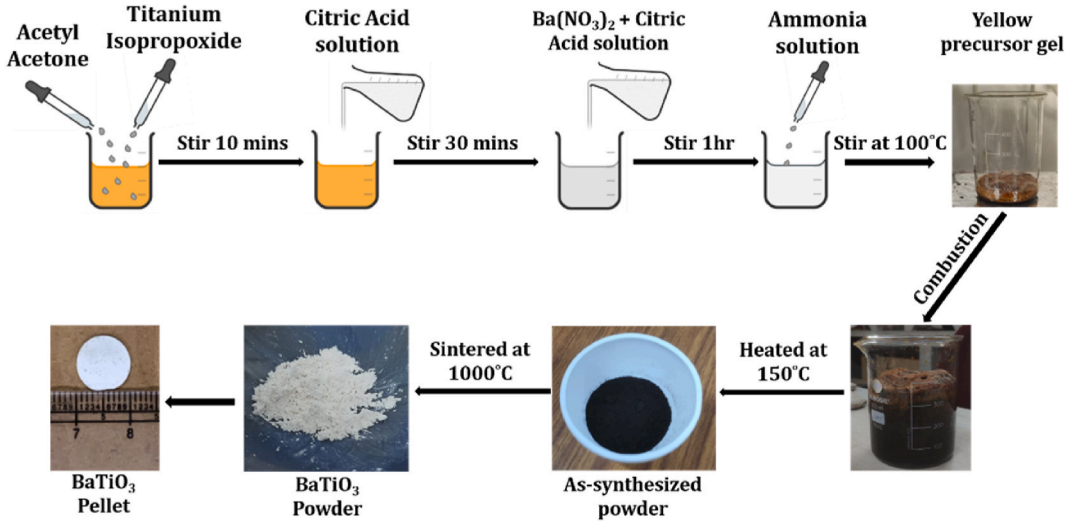

Fig. 1. Schematic diagram of the synthesis of tetragonal BT using citrate assisted sol-gel technique.

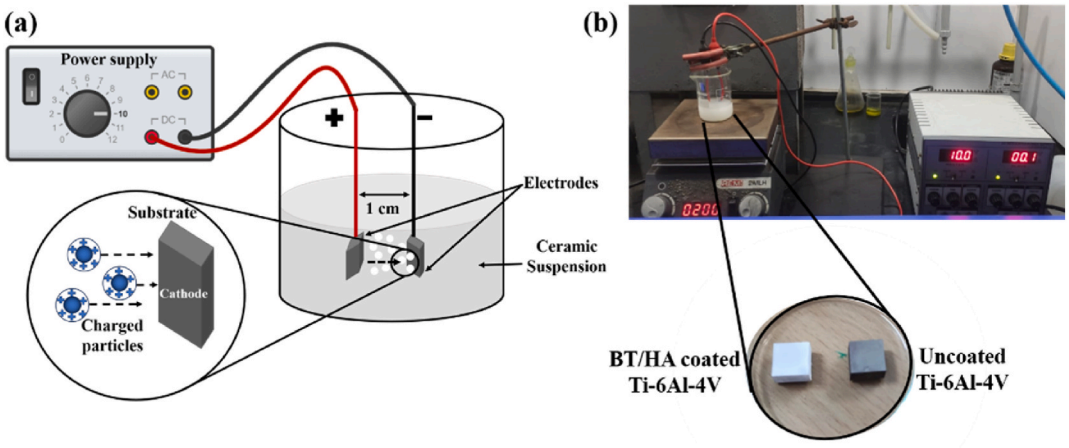

Fig. 2. (a) Schematic diagram of cathodic electrophoretic deposition of HA/BT composite on Ti-6Al-4V substrate & (b) laboratory set-up of the EPD technique and coated and uncoated substrate.

residue. Thus, the obtained sample was ground with mortar and pestle to homogenize the fine powder. To remove the organic substituent, the as-prepared powder was calcined at 450 °C for 5 h in an alumina crucible. The powder was further annealed at different temperatures i.e., 650, 850 and 1000 °C for 5 h each, followed by an intermediate grinding for each batch.

2.2. Preparation of BT/HA composite powder

Stoichiometric amounts of synthesized BT powder and commercially procured HA containing 40 %, 50 % and 60%wt BT (HB4, HB5 and HB6) were mixed in a mortar pestle by grinding continuously for 2 h. HA was acquired commercially from Medicoat, France. These composite powders were used for making the ceramic suspension for the EPD coatings. These powders were also uniaxially pressed into disks with a diameter of 10 mm and thickness of ~1 mm for d_{33} measurement and cell viability studies.

2.3. Electrophoretic deposition of BT/HA composite on Ti-6Al-4V

Ti-6Al-4V alloy with dimensions 10 mm × 10 mm x 5 mm were cut and polished with 200–1200 grit silicon carbide paper. These substrates were then ultrasonically degreased with acetone and distilled water and air dried. The Ti-6Al-4V alloys were used as both anode and cathode. The suspension was prepared with various BT/HA ratios of composite powders in 30 mL ethanol and ultrasonicating it for 30 min for stabilization. The powder to solvent ratio was determined after repeated trials, as explained in the supplementary section. A DC voltage of 10 V was applied across the electrodes immersed in the suspension for 10 min for all the coatings, these parameters were fixed after various trials. The laboratory set-up of the EPD technique is shown in Fig. 2(b). Conformal coatings were obtained which were air-dried for 24 h and subsequently vacuum sintered at 800 °C in steps of 10 °C/min for 2 h.

2.4. Characterizations

The crystal structure identification of the coatings was done by powder X-ray diffraction (XRD) analysis (Bruker D8 Advance, Germany) using a Cu-Kα radiation of wavelength 1.5406 Å. The phase confirmation was done using a Raman spectrometer (Horiba France LABRAM HR Evolution), fitted with ~532 nm laser. The morphology and elemental composition of the coated samples were analysed by scanning electron microscopy (SEM) technique (Carl Zeiss Evo/18) equipped with energy dispersive X-ray analysis (EDAX). The piezoelectric coefficient was measured using D33PZO1 d_{33} meter (Marine India). The surface hydrophilicity of the coated samples was measured using a contact angle measuring system (Holmarc Opto-Mechatronics Pvt. Ltd.). The hardness of the coatings was calculated using the Vicker's hardness tester (Mitutuoyo-HB210, Japan).

2.5. Cell viability studies

The conventional 3-(4,5-dimethylthiazol-2-yl)-2,5-diphenyl tetrazolium bromide (MTT) assay technique was used to evaluate the viability of HW-MSCs cell lines. HB4, HB5 and HB6 composite pellets with a diameter of 10 mm were used for the MTT assay. Human Wharton's jelly derived-mesenchymal stem cells (HW-MSCs) were purchased from Hi-Media, India, and were cultured in complete media of minimum essential medium alpha (MEM-α, Sigma) containing non-essential amino acids, sodium pyruvate, lipoic acid, vitamin B12, biotin and ascorbic acid, enriched with 10 % foetal bovine serum (FBS, Biological Industries) and 1 % penicillin/streptomycin (P/S, Biological Industries). The plates were incubated at 37 °C in a humidified atmosphere containing 5 % CO_2. For the following experiment, HW-MSCs passage 4 were utilized. Prior to performing *in vitro* experiments, the samples were cleaned in ethyl

alcohol and then sterilized using an autoclave. To perform cell viability assay, approximately 25,000 HW-MSCs cm^{-2} were seeded on the surface of samples in triplicate. As the control group, untreated wells were used without any sample addition. After the incubation for 48 h to promote cell adhesion, MTT assay was carried out according to the manufacturer's protocol (Sigma Aldrich). Post incubation, the pellets were separated from the solution and stop solution (10 % SDS in 0.01 N HCl) was introduced to dissolve the formazan crystals that were formed. The colorimetric readings were obtained at 595 nm using microplate absorbance reader (Thermo Multiskan FC).

3. Results and discussion

The crystallinity and the tetragonal phase of the powder samples and composite coatings were investigated using the XRD plots displayed in Fig. 3(a) & (b) respectively. A normal scan was carried out for all the samples with a step size of 0.0167° and scan time of 7 min. We observe that the composite powders and coatings are crystalline in nature as the XRD plot exhibits very sharp peaks. The peaks were indexed in reference to the standard values of ICDD 01-081-220 and 72–1243, for tetragonal BT and HA respectively. The split peak at $2\theta = 45°$corresponds to the (200) reflection in the tetragonal system. Due to the tetragonal crystal structure, the (200) plane of $BaTiO_3$ is twofold degenerate, which means that it has two equivalent orientations. These orientations result in two distinct diffraction peaks (002) and (200) that are symmetrically split around 45° in the XRD pattern [4]. The lattice constants for coatings are calculated using the equation for tetragonal crystal lattice as listed in Table 1, and the c/a values are found to be 1.0081, 1.0114 and 1.0091 for HB4, HB5 and HB6 powders respectively, which is well in accordance with the c/a value of 1.011, expected for tetragonal BT belonging to *P4mm* space group [16]. The equation to calculate lattice constant for tetragonal crystal lattice is as follows:

$$\frac{1}{d^2} = \frac{(h^2 + k^2)}{a^2} + \frac{l^2}{c^2} \tag{1}$$

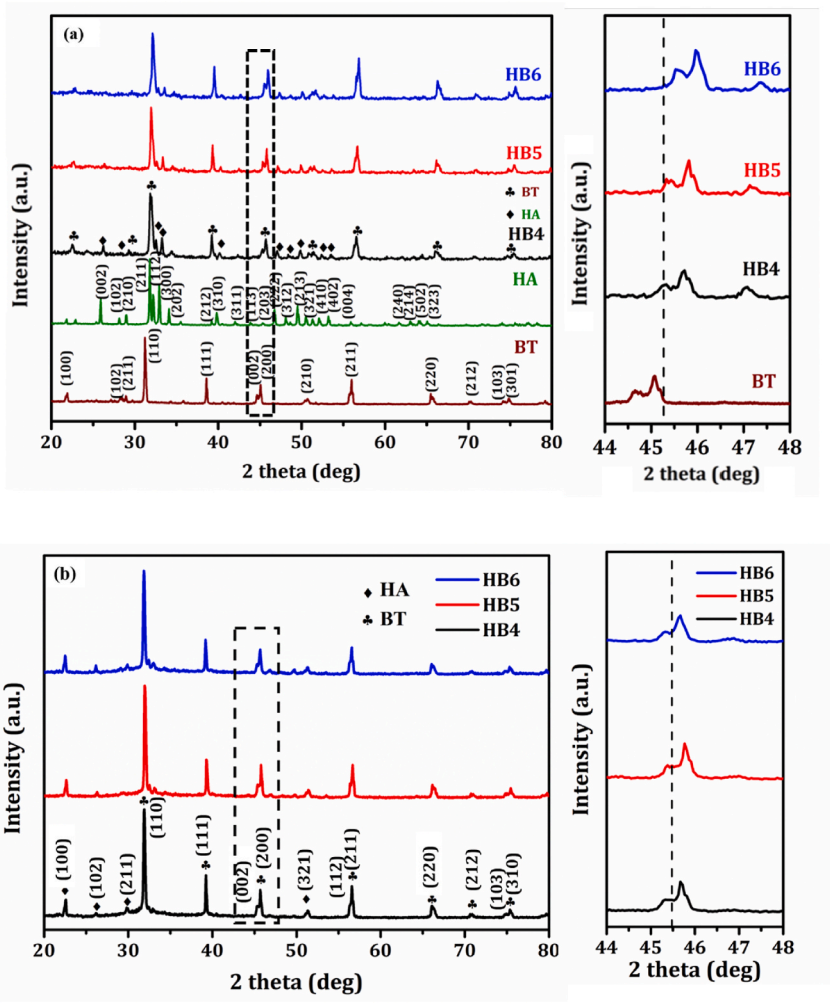

Fig. 3. XRD patterns of (a) pure HA, pure BT, and HB composite powders and (b) coatings; with a characteristic peak split at $2\theta \approx 45°$.

Table 1
Lattice parameters and c/a values of powder and coated samples.

Sample code	a (Å)	c (Å)	c/a	Structure Phase
BT	4.0199	4.0642	1.011	Tetragonal
HB4	3.9658	3.9981	1.0081	Tetragonal
HB5	3.9459	3.9819	1.0091	Tetragonal
HB6	3.9529	3.9981	1.0114	Tetragonal
HB4 (coating)	3.9658	3.9963	1.0077	Tetragonal
HB5 (coating)	3.9529	3.9981	1.0114	Tetragonal
HB6 (coating)	3.9459	4.0169	1.0180	Tetragonal

where d is the interplanar spacing, h,k,l are the miller indices and a, c are the lattice parameters.

In the case of the coated samples, the peak split around $2\theta \approx 45^{\circ}$ is remnant in all the samples as shown in Fig. 3(b), suggesting the piezoelectricity due to non-centrosymmetry in the crystal structure. The obtained XRD peaks suggest that there are no peaks corresponding to the Ti alloy substrate, as the coatings are having thickness in the range 10–60 μm as confirmed from the cross-section SEM analysis as well. From the XRD plot in Fig. 3(b), we can see that all the peaks are indexed in reference to standard values of ICDD 01-081-220 and 72–1243 for tetragonal BT and HA. The lattice constants were calculated and all the HB coatings exhibited c/a values nearing to the standard value of 1.0110 for tetragonal BT.

The tetragonal phase was further confirmed using the Raman spectra for all the HA/BT coatings. In the case of BT, the optical phonon modes show splitting of polar modes LO (longitudinal optical) and TO (transverse optical) in ferroelectric tetragonal phase. The broad bands around 260 cm^{-1} and 515 cm^{-1} corresponds to transverse optical modes of non-degenerate A_1 symmetry (A_1(TO)) due to Ti atom vibration in O_6-octahedron and the bending of Ti-O_6 octahedron respectively [17]. It is observed that all the composites show a red shift for 305 cm^{-1} band which is the characteristic band for tetragonal BT, with value going up to 319 cm^{-1} for the HB6 composite. This shift maybe due to compression of BT lattice by tensile strain because of the addition of bigger HA molecules to the HB composites. These bands confirms the ferroelectric phase arising due to the non-centrosymmetric tetragonal distortion of the off-centre Ti atoms of the Ti-O_6 octahedron assigned to the B_1 and degenerate E(TO + LO) modes [18]. The band at 717 cm^{-1} arises due the coupling between the tetragonal-phase dependent LO modes representing A_1(LO) and E(LO). Thus, a total number of 7 vibrational modes are identified and is represented by $\Gamma = 3A_1 + 4E + B_1$ [17,18]. All the composites exhibit bands around these points, confirming the tetragonality of the BT is intact. The band observed around 960 cm^{-1} attributes to the strong active υ1 Raman mode of P-O bond of HA [19,20]. The Raman spectra in Fig. 4 exhibits increasing intensity in the composite bands overlapping with the significant bands corresponding to the tetragonal BT and HA as well, thus affirmatively confirming the formation of the piezoelectric composites.

The SEM micrographs in Fig. 5(a,b,c) shows dense coatings on Ti-6Al-4V alloy, with the coatings becoming more uniform from HB4 to HB6. In general, the submicron-sized HA particles contribute to well-packed coatings [21]. The number of pores is decreasing as we increase the percentage of BT, exhibiting the best result for HB6. This improvement likely stems from barium titanate's lower surface energy, which enhances wetting and spreading on the Ti-6Al-4V substrate [22]. Additionally, the similar crystal structures of barium titanate and Ti-6Al-4V foster strong interfacial bonding between them and thus reduces the likelihood of defects, further contributing to the coating's uniformity and adhesion. The cross-section SEM image in Fig. 5(d,e,f) proves that the coatings are conformal, porous, and well attached to the substrate surface with coating thickness in the range of 10–60 μm.

The quantitative measurements of all the elemental compositions of the coating were approximately equal to the stoichiometric ratio of HA and BT and this confirmed the stability of the suspension. The EDAX analysis (Fig. 5(j)) reveals the elemental composition of the coatings. The analysis exhibits the presence of O, P, Ca of HA and O, Ti, Ba of BT respectively, and they are well in accordance with the composition of respective HB composites. The elemental mapping of HB4, HB5 and HB6 are observed in Fig. 5(g,h,i), and it

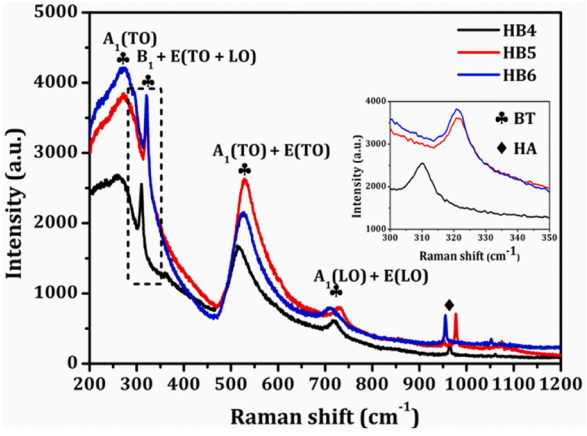

Fig. 4. Raman spectra of the HB coatings.

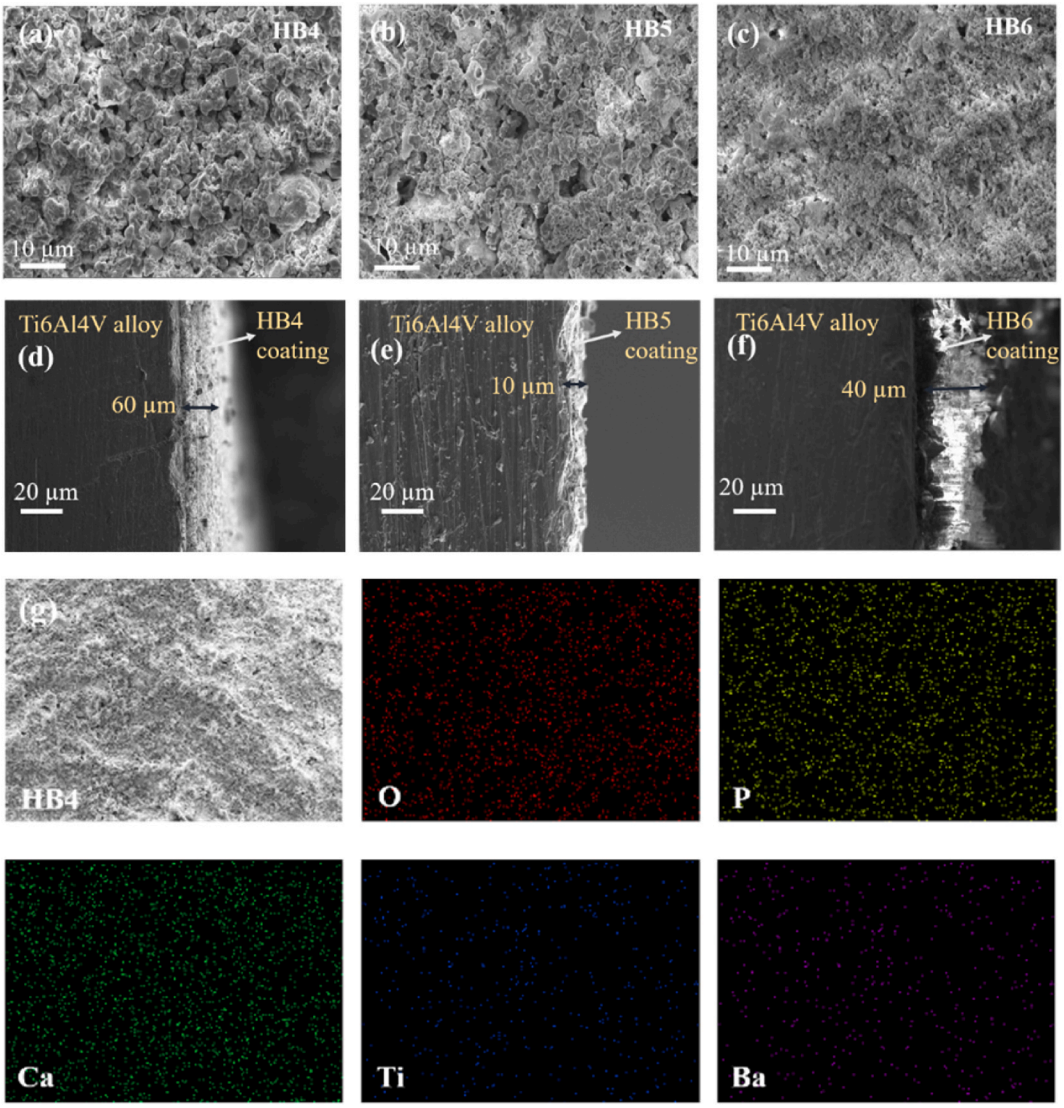

Fig. 5. Surface (a,b,c) and cross-section view (d,e,f) SEM micrographs of HB4, HB5, HB6 respectively; (g,h,i) elemental mapping of HB4, HB5 & HB6 and; (j) EDAX analysis of HB4, HB5, HB6.

further confirms that the coatings have been uniformly coated across the substrate, maintaining the composition intact.

It has been substantiated that surface coatings and modifications on implant metals can increase hydrophilicity, which in turn speeds up the osseointegration process [23]. Since high hydrophilicity tends to enhance cell adhesion and proliferation, contact angle values between 35° and 80° have been found to be ideal for materials in biomedical applications. Values below 35° adversely impair protein attachment, which is known to produce thrombogenicity [24–26]. The significant aspects influencing the surface features of implant coatings that should be considered are the alteration of the surface topography brought about by the newly deposited particles or molecules and their chemical interaction with proteins or water.

The contact angle values for the HB4, HB5 and HB6 coatings were obtained as 11.95°, 25.013° and 38.48°, respectively (Fig. 6(a,b, c)). It can be observed that with more HA concentration the coatings are highly hydrophilic owing to accelerated infiltration of water droplets by the HA molecules. The HB6 coating shows an optimum contact angle with water at 38.48°, which is much suited for cell adhesion and proliferation.

The Vicker's hardness studies were done on all the three coatings in a load range of 0.2–1.0 kgf for a dwell time of 10s, and the values are plotted as in Fig. 7. The Vicker's hardness (HV) was calculated using the following equation

$$\mathrm{HV} = 1.854\ \frac{F}{D^2}\ \left(\mathrm{kgf}\,/\,\mathrm{mm}^2\right) \tag{2}$$

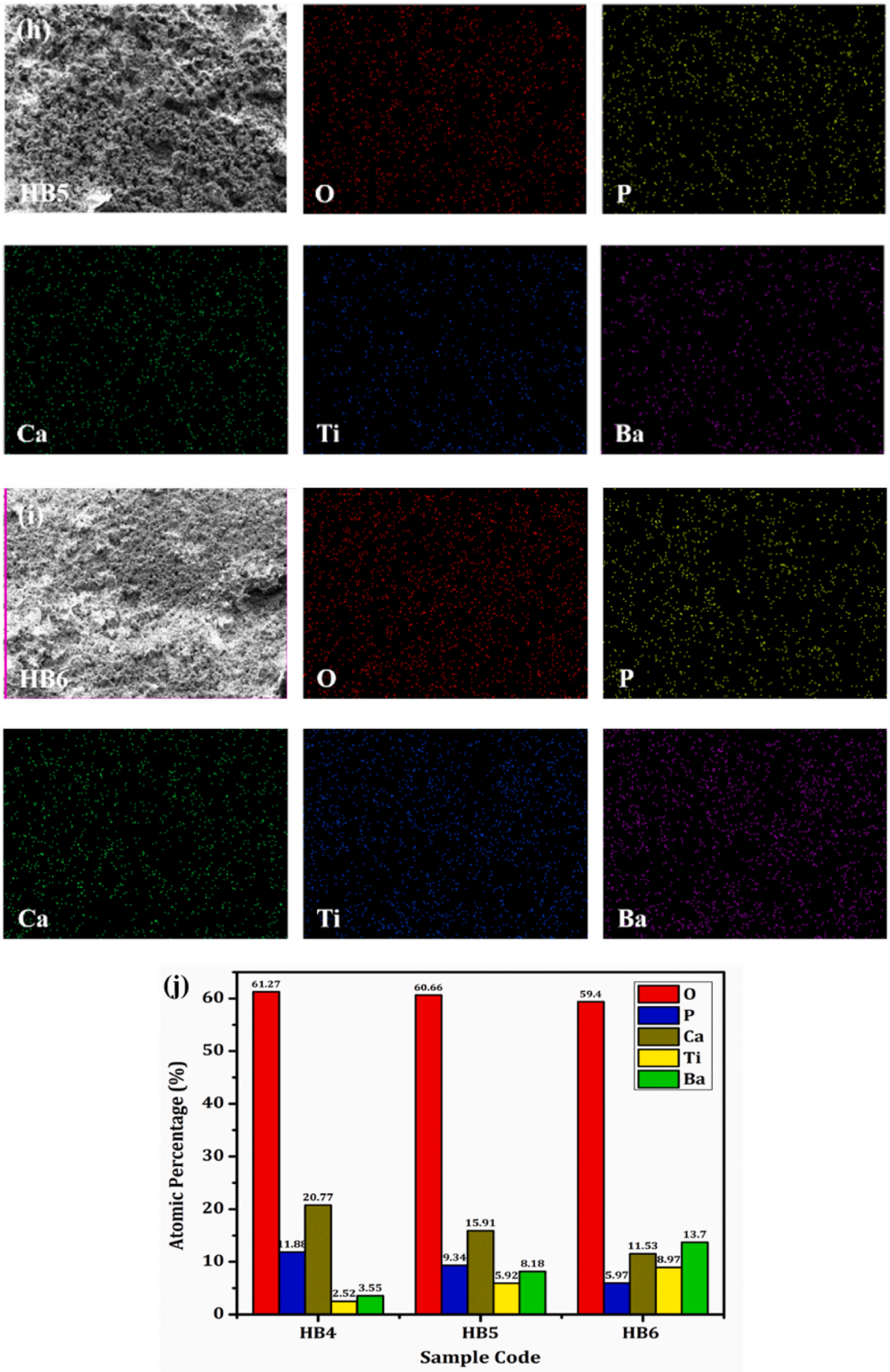

Fig. 5. (*continued*).

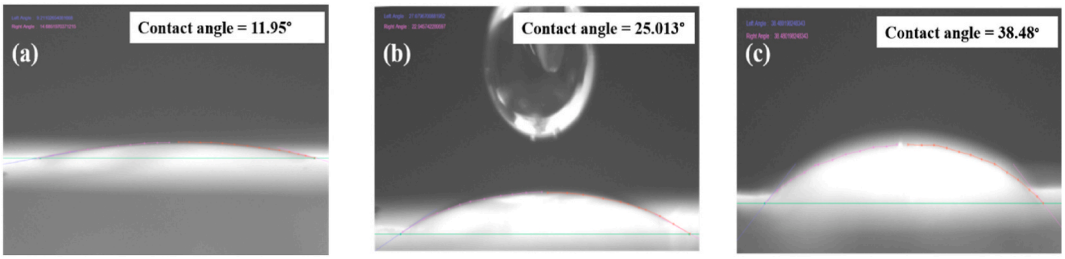

Fig. 6. Contact angle measurements of (a) HB4, (b) HB5 and (c) HB6 coatings.

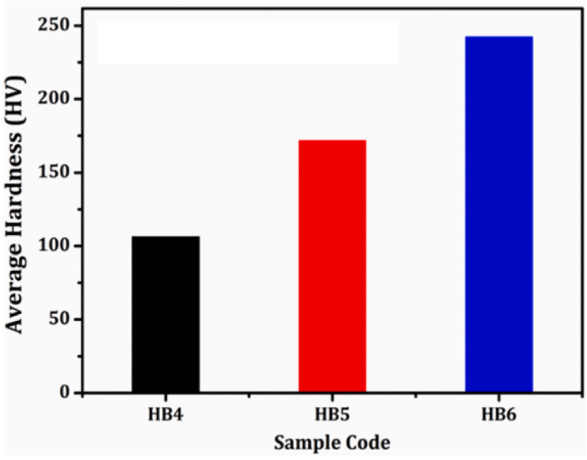

Fig. 7. Vicker's hardness plot for HB4, HB5 and HB6 coatings for a load range of 0.2–1.0 kgf.

where 1.854 is the Vicker's constant, F is the applied load in kgf and D^2 is the area of indentation in mm^2 [27]. It was observed that as the concentration of BT in HB composite was increased, the hardness of the coatings was increasing, with average hardness ranging from 106.13 HV, 171.88 HV and 242.31 HV for HB4, HB5 and HB6, respectively [28]. A study by Zysset et al. reports that natural human bone has a hardness ranging from 0.23 to 0.76 GPa. Their research suggests that incorporating BT at various weight percentages (40, 50 and 60 wt%) into a HA matrix increases the hardness beyond that of natural bone [29]. The study conducted by T. Webster et al. found that pure BT was the hardest material. This can be explained by the very strong attraction between barium and oxygen atoms in BT (over 562 kJ/mol). Stronger bonds require more energy to break. So, even a small amount of BT in the composite likely increases hardness because more energy is needed to break the bonds [30,31]. In the present work, HV value for HB6 was found to be highest owing to more amount of BT in it and this value lies closer to the desired range for a bone implant.

The composite pellets were subjected to poling at a voltage of 2 kV, for 4 h at 80 °C and then the d_{33} values were measured using a d_{33} meter. The measurement was carried out by setting the following parameters; 0.25 kN force, 110 Hz frequency, with an averaging of 100 samples/sec at room temperature. The obtained values are listed in Table 2 in comparison with pure BT and HA. It is observed that HB6 exhibits the maximum d_{33} coefficient among the composites, with a value of 159 pC/N.

Post the incubation (48 h), the cell viability of the samples were assessed using MTT assay. Subsequently, the percentage of cell viability was quantified using the following equation

$$\text{Cell Viability } \% = \frac{OD\ of\ test\ sample}{OD\ of\ control\ sample} \text{ X } 100 \tag{3}$$

where OD stands for the absorbance or optical density of UV light by the test and control samples [32].

The obtained cell viability percentage suggests that all the samples are biocompatible. The cell viability percentage for BT, HB4, HB5 and HB6 were obtained as 71.3 %, 72.4 %, 79.0 % and 91.7 % respectively. The variation in the cell compatibility for different HB compositions can be observed from fig. (8), suggesting that HB6 showcases the best cell viability. Thus, the *in vitro* studies concluded that the HB coatings do not release toxic substances and cause toxicity to the HW-MSCs.

4. Conclusion

In this study, we observe the formation of thick and conformal coatings of BT/HA composite over Ti-6Al-4V alloys through EPD technique. The addition of HA to BT creates tensile strains in BT leading to reduced bond lengths and improves crystallinity of the

Table 2
Piezoelectric coefficient values (d_{33}) of HB composite pellets.

Sample code	Density of pellet (g/cm^3)	d_{33} value (pC/N)
BT	3.999	168
HA	2.041	124
HB4	2.419	145
HB5	2.485	152
HB6	2.469	159

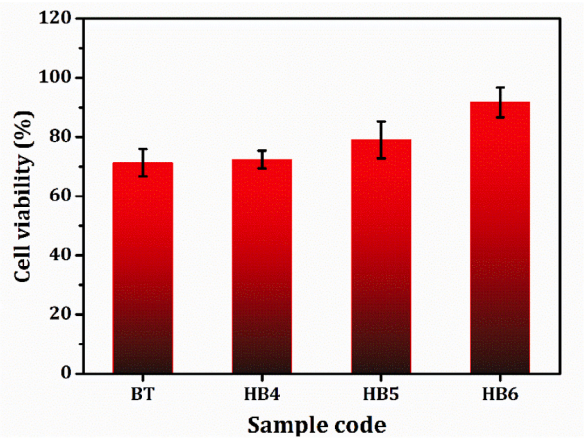

Fig. 8. Cytotoxicity profiles of BT, HB4, HB5 and HB6 for HW-MSCs cell lines.

composite, but it was also observed that if more than 40 % HA is added the desired properties tend to minimize. Thus, the HB6 composite exhibits better tetragonality, and therefore shows maximum d_{33} value of 159 pC/N. The SEM images and hardness studies also confirms that the HB6 composite showcases the most desirable properties for coating an orthopaedic implant. Overall, the present study evaluates the material and mechanical properties of the HB coatings on Ti alloy, which suggests that EPD is a promising technique for coating bioimplants. Additionally, the biocompatibility testing with human mesenchymal stem cells revealed that the HB6 sample had higher viability and there was negligible toxicity in all the other specimens. Further studies are to be carried out to evaluate the piezoelectric property of these coatings, to substantiate the possibility of improved osseointegration for bioimplants through piezoelectric ceramic coatings.

CRediT authorship contribution statement

Akhila S Nair: Writing – original draft, Visualization, Validation, Methodology, Investigation, Formal analysis, Data curation, Conceptualization. **Leema Rose Viannie:** Writing – review & editing, Supervision, Project administration.

Data availability

Data will be made available on request.

Declaration of competing interest

The authors declare that they have no known competing financial interests or personal relationships that could have appeared to influence the work reported in this paper.

Acknowledgements

The authors would like to express their sincere gratitude to VIT management for providing the 'VIT SEED' grant to carry out this work. The authors also thank Centre for Biomaterials, Cellular and Molecular Theranostics (CBCMT), VIT for helping with the characterization facilities.

Appendix A. Supplementary data

Supplementary data to this article can be found online at https://doi.org/10.1016/j.heliyon.2024.e39102.

References

[1] C. Polley, T. Distler, R. Detsch, H. Lund, A. Springer, A.R. Boccaccini, H. Seitz, 3D printing of piezoelectric barium titanate-hydroxyapatite scaffolds with interconnected porosity for bone tissue engineering, Materials 13 (2020) 1–16, https://doi.org/10.3390/MA13071773.

[2] I. Fukada, E. y Yasuda, On the piezoelectric of Bone.Pdf, J. Phys. Soc. Japan 12 (1957).

[3] A. Ehterami, M. Kazemi, B. Nazari, P. Saraeian, M. Azami, Fabrication and characterization of highly porous barium titanate based scaffold coated by Gel/HA nanocomposite with high piezoelectric coefficient for bone tissue engineering applications, J. Mech. Behav. Biomed. Mater. 79 (2018) 195–202, https://doi.org/10.1016/j.jmbbm.2017.12.034.

[4] M. Prakasam, M. Albino, E. Lebraud, M. Maglione, C. Elissalde, A. Largeteau, Hydroxyapatite-barium titanate piezocomposites with enhanced electrical properties, J. Am. Ceram. Soc. 100 (2017) 2621–2631, https://doi.org/10.1111/jace.14801.

[5] L. Mohan, D. Durgalakshmi, M. Geetha, T.S.N. Sankara Narayanan, R. Asokamani, Electrophoretic deposition of nanocomposite (HAp + TiO 2) on titanium alloy for biomedical applications, Ceram. Int. 38 (2012) 3435–3443, https://doi.org/10.1016/j.ceramint.2011.12.056.

[6] B. Fan, Z. Guo, X. Li, S. Li, P. Gao, X. Xiao, J. Wu, C. Shen, Y. Jiao, W. Hou, Electroactive barium titanate coated titanium scaffold improves osteogenesis and osseointegration with low-intensity pulsed ultrasound for large segmental bone defects, Bioact. Mater. 5 (2020) 1087–1101, https://doi.org/10.1016/j.bioactmat.2020.07.001.

[7] X. Pang, T. Wang, B. Liu, X. Fan, X. Liu, J. Shen, C. Zhong, W. Hu, Effect of solvents on the morphology and structure of barium titanate synthesized by a one-step hydrothermal method, Int. J. Miner. Metall. Mater. 30 (2023) 1407–1416, https://doi.org/10.1007/s12613-023-2614-9.

[8] M. Inada, N. Enomoto, K. Hayashi, J. Hojo, S. Komarneni, Facile synthesis of nanorods of tetragonal barium titanate using ethylene glycol, Ceram. Int. 41 (2015) 5581–5587, https://doi.org/10.1016/j.ceramint.2014.12.137.

[9] K. Hongo, S. Kurata, A. Jomphoak, M. Inada, K. Hayashi, R. Maezono, Stabilization mechanism of the tetragonal structure in a hydrothermally synthesized BaTiO3 nanocrystal, Inorg. Chem. 57 (2018) 5413–5419, https://doi.org/10.1021/acs.inorgchem.8b00381.

[10] W. Liu, X. Li, Y. Jiao, C. Wu, S. Guo, X. Xiao, X. Wei, J. Wu, P. Gao, N. Wang, Y. Lu, Z. Tang, Q. Zhao, J. Zhang, Y. Tang, L. Shi, Z. Guo, Biological effects of a three-dimensionally printed Ti6Al4V scaffold coated with piezoelectric BaTiO3Nanoparticles on bone formation, ACS Appl. Mater. Interfaces 12 (2020) 51885–51903, https://doi.org/10.1021/acsami.0c10957.

[11] A. Sobolev, I. Wolicki, A. Kossenko, M. Zinigrad, K. Borodianskiy, Coating formation on Ti-6Al-4V alloy by Micro Arc Oxidation in molten salt, Materials 11 (2018) 4–11, https://doi.org/10.3390/ma11091611.

[12] P. Hameed, V. Gopal, S. Bjorklund, A. Ganvir, D. Sen, N. Markocsan, G. Manivasagam, Axial Suspension Plasma Spraying: an ultimate technique to tailor Ti6Al4V surface with HAp for orthopaedic applications, Colloids Surfaces B Biointerfaces 173 (2019) 806–815, https://doi.org/10.1016/j.colsurfb.2018.10.071.

[13] C.E. Wen, W. Xu, W.Y. Hu, P.D. Hodgson, Hydroxyapatite/titania sol-gel coatings on titanium-zirconium alloy for biomedical applications, Acta Biomater. 3 (2007) 403–410, https://doi.org/10.1016/j.actbio.2006.10.004.

[14] Motahareh Sinaei, F. Heidari, R. Hayati, Investigation of corrosion properties of nano-composite coatings of hydroxyapatite/barium titanate/chitosan produced by electrophoretic deposition on 316L stainless steel, Surf. Eng. Appl. Electrochem. 56 (2020) 272–281, https://doi.org/10.3103/S1068375520030175.

[15] J. Krčil, Z. Rafaj, V. Mára, S. Krum, V. Starý, V. Nehasil, J. Sobotová, The analysis of thermal and anodic oxide layers on selected biocompatible titanium alloys, Surf. Interface Anal. 50 (2018) 1007–1011, https://doi.org/10.1002/sia.6466.

[16] W. Sun, C. Li, J. Li, W. Liu, Microwave-hydrothermal synthesis of tetragonal BaTiO3 under various conditions, Mater. Chem. Phys. 97 (2006) 481–487, https://doi.org/10.1016/j.matchemphys.2005.08.051.

[17] V. Dwij, B.K. De, G. Sharma, D.K. Shukla, M.K. Gupta, R. Mittal, V. Sathe, Revisiting 70 Years of Lattice Dynamics of BaTiO3: Combined First Principle and Experimental Investigation, vol. 1, 2020, pp. 1–16. http://arxiv.org/abs/2012.12669.

[18] T. Wang, X. Pang, B. Liu, J. Liu, J. Shen, C. Zhong, A facile and eco-friendly hydrothermal synthesis of high tetragonal barium titanate with uniform and controllable particle size, Materials 16 (2023), https://doi.org/10.3390/ma16114191.

[19] M. Głąb, S. Kudłacik-Kramarczyk, A. Drabczyk, A. Kordyka, M. Godzierz, P.S. Wróbel, A. Tomala, B. Tyliszczak, A. Sobczak-Kupiec, Evaluation of the impact of pH of the reaction mixture, type of the stirring, and the reagents' concentration in the wet precipitation method on physicochemical properties of hydroxyapatite so as to enhance its biomedical application potential, J. Biomed. Mater. Res. Part B Appl. Biomater. 110 (2022) 2649–2666, https://doi.org/10.1002/jbm.b.35118.

[20] J.A. Stammeier, B. Purgstaller, D. Hippler, V. Mavromatis, M. Dietzel, In-situ Raman spectroscopy of amorphous calcium phosphate to crystalline hydroxyapatite transformation, MethodsX 5 (2018) 1241–1250, https://doi.org/10.1016/j.mex.2018.09.015.

[21] C.T. Kwok, P.K. Wong, F.T. Cheng, H.C. Man, Characterization and corrosion behavior of hydroxyapatite coatings on Ti6Al4V fabricated by electrophoretic deposition, Appl. Surf. Sci. 255 (2009) 6736–6744, https://doi.org/10.1016/j.apsusc.2009.02.086.

[22] D. Padalia, U. Kumar, P. Bhandari, J. Dalal, L. Ranakoti, T. Singh, Tuning the structural, optical, and dielectric properties of europium-doped barium titanate ceramics, J. Mater. Sci. Mater. Electron. 35 (2024) 1–22, https://doi.org/10.1007/s10854-024-12984-9.

[23] K.A. Kravanja, M. Finšgar, Analytical techniques for the characterization of bioactive coatings for orthopaedic implants, Biomedicines 9 (2021), https://doi.org/10.3390/biomedicines9121936.

[24] E. Avcu, Y. Yıldıran Avcu, F.E. Baştan, M.A.U. Rehman, F. Üstel, A.R. Boccaccini, Tailoring the surface characteristics of electrophoretically deposited chitosan-based bioactive glass composite coatings on titanium implants via grit blasting, Prog. Org. Coatings 123 (2018) 362–373, https://doi.org/10.1016/j.porgcoat.2018.07.021.

[25] Q. Chen, S. Cabanas-Polo, O.M. Goudouri, A.R. Boccaccini, Electrophoretic co-deposition of polyvinyl alcohol (PVA) reinforced alginate-Bioglass® composite coating on stainless steel: mechanical properties and in-vitro bioactivity assessment, Mater. Sci. Eng. C 40 (2014) 55–64, https://doi.org/10.1016/j.msec.2014.03.019.

[26] F. Gebhardt, S. Seuss, M.C. Turhan, H. Hornberger, S. Virtanen, A.R. Boccaccini, Characterization of electrophoretic chitosan coatings on stainless steel, Mater. Lett. 66 (2012) 302–304, https://doi.org/10.1016/j.matlet.2011.08.088.

[27] Aminatun, F.F.S.B. Tenong, D. Hikmawati, E.M. Setiawati, Characterization of vickers hardness and corrosion rate of stainless steel-316L coated with hydroxyapatite-polyvinyl alcohol, J. Phys. Conf. Ser. 1816 (2021), https://doi.org/10.1088/1742-6596/1816/1/012012.

[28] N. Asgari, M. Rajabi, Enhancement of mechanical properties of hydroxyapatite coating prepared by electrophoretic deposition method, Int. J. Appl. Ceram. Technol. 18 (2021) 147–153, https://doi.org/10.1111/ijac.13638.

[29] P.K. Zysset, X. Edward Guo, C. Edward Hoffler, K.E. Moore, S.A. Goldstein, Elastic modulus and hardness of cortical and trabecular bone lamellae measured by nanoindentation in the human femur, J. Biomech. 32 (1999) 1005–1012, https://doi.org/10.1016/S0021-9290(99)00111-6.

[30] M. Tavangar, F. Heidari, R. Hayati, F. Tabatabaei, D. Vashaee, L. Tayebi, Manufacturing and characterization of mechanical, biological and dielectric properties of hydroxyapatite-barium titanate nanocomposite scaffolds, Ceram. Int. 46 (2020) 9086–9095, https://doi.org/10.1016/j.ceramint.2019.12.157.

[31] T.J. Webster, C. Ergun, R.H. Doremus, R.W. Siegel, R. Bizios, Enhanced functions of osteoblasts on nanophase ceramics, Biomaterials 21 (2000) 1803–1810, https://doi.org/10.1016/S0142-9612(00)00075-2.

[32] A. Almutary, B.J.S. Sanderson, The MTT and crystal violet assays: potential confounders in nanoparticle toxicity testing, Int. J. Toxicol. 35 (2016) 454–462, https://doi.org/10.1177/1091581816648906.